Journal of Experimental Botany
doi:10.1093/jxb/eraa583 Advance Access Publication 14 December, 2020

RESEARCH PAPER

Proteolytic cleavage of *Arabidopsis thaliana* phospho*enol*pyruvate carboxykinase-1 modifies its allosteric regulation

Bruno E. Rojas, Matías D. Hartman*, Carlos M. Figueroa and Alberto A. Iglesias†

Instituto de Agrobiotecnología del Litoral, UNL, CONICET, FBCB, Santa Fe, Argentina

* Present address: Max Planck Institute for Biology of Ageing, Cologne, Germany.
† Correspondence: iglesias@fbcb.unl.edu.ar

Received 29 July 2020; Editorial decision 3 December 2020; Accepted 10 December 2020

Editor: Daniel Gibbs, University of Birmingham, UK

Abstract

Phospho*enol*pyruvate carboxykinase (PEPCK) plays a crucial role in gluconeogenesis. In this work, we analyze the proteolysis of *Arabidopsis thaliana* PEPCK1 (*Ath*PEPCK1) in germinating seedlings. We found that the amount of *Ath*PEPCK1 protein peaks at 24–48 h post-imbibition. Concomitantly, we observed shorter versions of *Ath*PEPCK1, putatively generated by metacaspase-9 (*Ath*MC9). To study the impact of *Ath*MC9 cleavage on the kinetic and regulatory properties of *Ath*PEPCK1, we produced truncated mutants based on the reported *Ath*MC9 cleavage sites. The Δ19 and Δ101 truncated mutants of *Ath*PEPCK1 showed similar kinetic parameters and the same quaternary structure as the wild type. However, activation by malate and inhibition by glucose 6-phosphate were abolished in the Δ101 mutant. We propose that proteolysis of *Ath*PEPCK1 in germinating seedlings operates as a mechanism to adapt the sensitivity to allosteric regulation during the sink-to-source transition.

Keywords: *Arabidopsis thaliana*, gluconeogenesis, metacaspase, phospho*enol*pyruvate carboxykinase, proteolysis, seedlings.

Introduction

Phospho*enol*pyruvate (PEP) is a metabolic hub that connects various pathways, including glycolysis, gluconeogenesis, and metabolism of organic and amino acids (Chiba *et al.*, 2015). Among the enzymes that metabolize PEP, phospho*enol*pyruvate carboxykinase (PEPCK) is particularly relevant, due to its numerous physiological functions (Leegood and Walker, 2003; Latorre-Muro *et al.*, 2018; Wang and Dong, 2019). Based on the phosphate donor, PEPCKs are classified as ATP (EC 4.1.1.49), GTP (EC 4.1.1.32), or PPi dependent (EC 4.1.1.38), all with different evolutionary origin (Matte *et al.*, 1997; Fukuda *et al.*, 2004; Aich and Delbaere, 2007; Chiba *et al.*, 2015).

ATP-dependent PEPCK is found in bacteria, yeasts, and plants. This enzyme catalyzes the reversible decarboxylation of oxaloacetate (OAA) to form PEP, according to the reaction: $OAA+ATP \leftrightarrow PEP+ADP+CO_2$. Although this reaction is fully reversible *in vitro*, it is generally accepted that it proceeds

Abbreviations: *Ath*MC9, *Arabidopsis thaliana* metacaspase-9; *Ath*PEPCK1, *Arabidopsis thaliana* phospho*enol*pyruvate carboxykinase-1; Glc6P, glucose 6-phosphate; OAA, oxaloacetic acid; PEP, phospho*enol*pyruvate; PPi, inorganic pyrophosphate.

towards OAA decarboxylation *in vivo* (Johnson *et al.*, 2016). PEPCK requires two divalent cations to catalyze the reaction: one Mn^{2+} ion which acts as an essential activating cofactor that promotes OAA decarboxylation and stabilizes the enolate ion during catalysis and one Mg^{2+} cation which forms the metal nucleotide complex that constitutes the active form of the substrate (Goldie and Sanwal, 1980; Burnell, 1986; Matte *et al.*, 1997; Johnson *et al.*, 2016).

ATP-dependent PEPCK is a cytosolic enzyme (Ito *et al.*, 2011; Tsiatsiani *et al.*, 2013) with different physiological roles in plants: (i) it is part of the CO_2-concentrating mechanisms operating in C_4 and Crassulacean acid metabolism (CAM) photosynthesis (Edwards *et al.*, 1971; Reiskind and Bowes, 1991; Martín *et al.*, 2011); (ii) it participates in biotic and abiotic stress responses (Sáez-Vásquez *et al.*, 1995; Chen *et al.*, 2000, 2002; Saito *et al.*, 2008; Penfield *et al.*, 2012; Choi *et al.*, 2015); (iii) it is involved in nitrogen and amino acid metabolism, especially during fruit development (Walker *et al.*, 1999; Lea *et al.*, 2001); and (iv) it is involved in gluconeogenesis during seed germination, channeling carbon released from fatty acid reserves to form sugars, until the photosynthetic apparatus is fully developed (Rylott *et al.*, 2003; Penfield *et al.*, 2004; Malone *et al.*, 2007; Graham, 2008; Eastmond *et al.*, 2015).

The occurrence and regulatory effects of proteolysis on PEPCK have remained obscure. Walker *et al.* (1995) found that a discrete proteolytic cleavage at the N-terminus of PEPCK occurred in crude extracts from cucumber cotyledons and leaves of C_4 and CAM species; however, proteolysis of the cucumber PEPCK did not significantly alter its activity (Walker and Leegood, 1995). Two PEPCK isoforms of different molecular mass (74 kDa and 65 kDa) were found in *Ananas comosus* (pineapple) leaves. The shorter version was purified to homogeneity and biochemically characterized, but study of the large isoform was not possible because it was recalcitrant to purification (Martín *et al.*, 2011).

A large-scale study conducted by Tsiatsiani *et al.* (2013) identified *Ath*PEPCK1 as a substrate of *Arabidopsis thaliana* (Arabidopsis) metacaspase-9 (*Ath*MC9). This cysteine protease cleaved *Ath*PEPCK1 at the N-terminus, which seemed to boost PEPCK activity. In crude extracts, PEPCK activity was reduced in the *mc9* mutant and increased in the MC9-overexpressing lines (Tsiatsiani *et al.*, 2013). *Ath*MC9 is localized in the nucleus, cytosol, and apoplast (Vercammen *et al.*, 2006; Kwon and Hwang, 2013; Tsiatsiani *et al.*, 2013), and is implicated in cell death regulation in many physiological situations, for example during plant immune response (Kim *et al.*, 2013; Shen *et al.*, 2019) and plant vascular development (Escamez *et al.*, 2016, 2019).

Arabidopsis has two *ATP-PEPCK* genes, *pck1* (AT4G37870) and *pck2* (AT5G65690), encoding *Ath*PEPCK1 and *Ath*PEPCK2, respectively. We have recently reported the biochemical properties of these proteins, which are finely regulated by numerous metabolites. Mainly, they are inhibited by glucose 6-phosphate (Glc6P), shikimate, and inorganic pyrophosphate (PPi), and activated by malate (Rojas *et al.*, 2019). In this work, we focused on the combined effects of allosteric regulation and proteolysis on the activity of *Ath*PEPCK1, which plays a critical role during seed germination (Rylott *et al.*, 2003; Penfield *et al.*, 2004). We used recombinant proteins to study in detail the biochemical effects of the *Ath*MC9-mediated cleavage of *Ath*PEPCK1. Our results show that proteolysis of the N-terminus modifies the allosteric regulation of *Ath*PEPCK1, which could have important metabolic implications during the sink-to-source transition associated with seedling development.

Materials and methods

Reagents

ATP, ADP, PEP, OAA, NADH, Glc6P, L-malic acid, pyruvate kinase, and L-malic dehydrogenase were from Sigma Aldrich. L-Lactate dehydrogenase was from Roche. All other reagents were of the highest available quality.

Plant material and growth conditions

All experiments were performed with Arabidopsis Col-0. The *pck1* mutant corresponds to the SALK_072899C T-DNA insertion. Seeds were disinfected with 70% (v/v) ethanol for 5 min, then treated with 10% (v/v) bleach for 10 min and washed three times with sterile, distilled water. Seeds were soaked in sterile 0.1% (w/v) agar and stratified at 4 °C in the dark for 2 d. In germinating assays, seeds were sown on a mesh soaked with 0.5× Murashige and Skoog medium in 16 cm diameter Petri dishes and transferred to growth chambers (Raineri *et al.*, 2016). In mature leaf assays, plants were grown on soil in 8 cm diameter×7 cm height pots, one plant per pot. In all cases, plants were grown at 23 °C and 120 µmol m^{-2} s^{-1}, with a long-day photoperiod (16 h light and 8 h dark). The seeds employed were harvested, dried in darkness at room temperature, and stored at 4 °C. In all experiments, samples were taken, immediately frozen with liquid nitrogen, and stored at –80 °C until use.

Protein extraction

Plant material was homogenized in a pre-cooled mortar with liquid nitrogen. For denaturing protein extraction, 20 mg of FW tissue was extracted with 200 µl of denaturing sample buffer, consisting of 2% (w/v) SDS, 20% (w/v) glycerol, 1.4 M 2-mercaptoethanol, 125 mM Tris–HCl pH 6.8, and 0.05% (w/v) bromophenol blue. After adding the buffer, samples were vortexed and heated for 5 min at 95 °C with agitation. Samples were cooled to room temperature and centrifuged at 21 000 *g* for 10 min to separate the protein extract from tissue debris. For ultra-denaturing protein extraction, 20 mg of FW tissue were extracted with 10% (w/v) trichloroacetic acid (TCA) (Wu and Wang, 1984) or with 10% (w/v) TCA in acetone (Isaacson *et al.*, 2006). For native protein extraction, 20 mg of FW tissue was extracted with 500 µl of native buffer, consisting of 100 mM Bicine-KOH pH 9.0, 10% (v/v) glycerol, 0.1% (v/v) Triton X-100, 5 mM 2-mercaptoethanol, 1 mM EDTA, 1 mM EGTA, 1 mM benzamidine, 1 mM ε-aminocapronic acid, 2 mM phenylmethylsulfonyl fluoride (PMSF), 1× Set III protease cocktail (Merck, 539134), 1 mM NaF, 1 mM Na_2MO_4, and 1 mM Na_3VO_4. After adding the extraction buffer, samples were vortexed and incubated on ice for 10 min and then centrifuged at 21 000 *g* for 10 min. Then, the protein extract was separated from tissue debris and transferred to a new tube.

Production and purification of recombinant proteins

The production of recombinant *Ath*PEPCK1 was performed as previously described (Rojas *et al.*, 2019). The sequence coding for *Ath*MC9 (At5g04200) was cloned using cDNA from Arabidopsis seedlings with the primers *Ath*MC9-fo (GGATCCGATGGATCAACAAGGGATGG TCAAG, the *Bam*HI site is underlined) and *Ath*MC9-re (GAATTCTC AAGGTTGAGAAAGGAACGTCG, the *Eco*RI site is underlined). The amplified sequence was inserted in-frame with an N-terminal His_6-tag between the *Bam*HI and *Eco*RI sites of the pETDuet-1 vector (Novagen). Protein expression was performed in *Escherichia coli* BL21 (DE3) (Invitrogen) grown in LB medium supplemented with 100 μg ml^{-1} ampicillin and induced with 0.5 mM isopropyl-β-D-1-thiogalactopyranoside for 16 h at 18 °C with agitation. Cells were harvested by centrifugation and resuspended in lysis buffer [25 mM Tris–HCl pH 8.0, 300 mM NaCl, 5% (v/v) glycerol, and 10 mM imidazole]. Cells were disrupted by sonication and centrifuged at 12 000 *g* for 15 min at 4 °C. The crude extract was loaded on an IDA-Ni^{2+} column, previously equilibrated with lysis buffer. The recombinant protein was eluted with lysis buffer supplemented with 300 mM imidazole and 10% (v/v) glycerol.

Production of antisera

Polyclonal antibodies against *Ath*PEPCK1 were raised in rabbits using the purified recombinant protein at the Centro de Medicina Comparada (ICIVET Litoral, CONICET-UNL, Argentina). To further increase the specificity, the antiserum was purified with *Ath*PEPCK1, following a previously described protocol (Fang, 2012). Polyclonal antibodies against *Titricum aestivum* NAD-dependent glyceraldehyde-3-phosphate dehydrogenase (*Tae*GAPDH) were produced by Piattoni *et al.* (2017).

Protein methods

Total proteins were quantified with the Bradford assay (Bradford, 1976), using a standard curve constructed with BSA.

Protein electrophoresis was performed under denaturing conditions (SDS–PAGE), according to the method described by Laemmli (1970). For immunodetection, proteins were transferred to 0.45 μm nitrocellulose membranes (Amersham) at 180 mA for 60 min. Membranes were incubated overnight at 4 °C with purified anti-*Ath*PEPCK1 antibodies diluted 1:1000 and then incubated for 1 h at room temperature with goat anti-rabbit IgG H&L conjugated to horseradish peroxidase (Abcam, ab6721) diluted 1:10 000. Protein bands were revealed with SuperSignal West Pico Plus Chemiluminescent Substrate (Thermo Fischer Scientific), following the manufacturer's instructions. Radiographic films (AGFA) were exposed for between 2.5 min and 5 min for the detection of *Ath*PEPCK1. Antibodies were stripped with 100 mM glycine pH 2.5 to analyze protein loading. Membranes were thoroughly washed and then incubated overnight with anti-*Tae*GAPDH antibodies diluted 1:5000. All subsequent steps were performed as previously described. In this case, exposure times were between 30 s and 1 min.

Enzyme activity assays

Recombinant *Ath*PEPCK1 and the Δ19 and Δ101 truncated mutants were assayed spectrophotometrically as previously described (Rojas *et al.*, 2019), with the concentrations of substrates indicated below.

Carboxylase activity of PEPCK in crude extracts was measured using 100 mM HEPES-NaOH pH 7.0, 4 mM 2-mercaptoethanol, 0.2 mM NADH, 4 mM $MgCl_2$, 1 mM $MnCl_2$, 100 mM $KHCO_3$, 0.2 mM ADP, 10 mM PEP, and 1 U of malate dehydrogenase. Assays were performed in 250 μl at 30 °C and were corrected for PEP carboxylase activity by omitting ADP from the reaction mixture, as previously done by Martín *et al.* (2007). Activity was calculated by measuring the change in absorbance at 340 nm due to NADH consumption.

Kinetic parameters were calculated using the software GraphPad Prism (Version 5). Activity data were plotted against the concentration of the variable substrate or effector and fitted to a modified Hill equation: $v=v_0+(V-v_0)\times C^{nH}/(k^{nH}+C^{nH})$, where v is the initial velocity; v_0 is the velocity in the absence of the substrate or effector being analyzed; V is the maximal velocity (V_{max}), activation or inhibition; C is the concentration of substrate or effector under study; k is the concentration of substrate or effector producing half of the maximal velocity (K_m), activation ($A_{0.5}$) or inhibition ($I_{0.5}$); and n_H is the Hill coefficient. Substrate kinetic parameters were calculated fixing the n_H to 1, which turns the modified Hill equation into the classical Michaelis–Menten equation.

One unit is defined as the amount of enzyme that catalyzes the formation of 1 μmol of product (PEP or OAA) per minute under the specified assay conditions (of decarboxylation or carboxylation, respectively). Allosteric effectors were assayed under standard conditions (see above). Before performing these experiments, effectors were tested on coupled enzymes to avoid unwanted effects.

Recombinant *Ath*MC9 protein was assayed as described previously by Vercammen *et al.* (2004), with minor modifications. Reactions were done with 50 mM MES-KOH pH 5.5, 150 mM NaCl, 300 mM sucrose, 10 mM DTT, 0.3 μg μl^{-1} *Ath*MC9, and 0.15 μg μl^{-1} *Ath*PEPCK1. Aliquots were taken at different time intervals and analyzed by SDS–PAGE and PEPCK activity.

Native molecular mass determination

Protein molecular mass was determined by gel filtration chromatography using a Superdex 200 10/300 column (GE Healthcare) equilibrated with 50 mM HEPES pH 8.0 and 100 mM NaCl. A calibration curve was constructed by plotting K_{av} values versus log(molecular mass) of protein standards, including thyroglobulin (669 kDa), ferritin (440 kDa), aldolase (158 kDa), conalbumin (75 kDa), ovalbumin (44 kDa), carbonic anhydrase (29 kDa), and RNase (13.7 kDa). K_{av} values were calculated as $(V_e-V_0)/(V_t-V_0)$, where V_e is the elution volume of the protein, V_0 is the elution volume of dextran blue (Promega), and V_t is the total volume of the column.

Protein thermal shift assays

Protein thermal shift assays were performed as previously described (Rojas *et al.*, 2019). Assays were performed in a final volume of 20 μl with 0.15 mg ml^{-1} protein, 4× Sypro Orange (Sigma), and 25 mM HEPES-NaOH pH 7.0 in MicroAmp fast 96-well PCR plates (Applied Biosystems). All the reactions were performed with their corresponding controls (without protein or effector). Plates were sealed with Microseal adhesive film (Bio-Rad) and heated in a StepOne Real-Time PCR System (Applied Biosystems) from 25 °C to 99 °C, with increments of 0.4 °C. Changes in fluorescence were monitored simultaneously. The wavelengths for excitation and emission were 490 nm and 575 nm, respectively. The melting temperature (T_m) of each sample was calculated by plotting the first derivative of the fluorescence emission ($-dF/dT$) as a function of temperature (T) and identifying the minimum of the curve. The shift in the melting temperature (ΔT_m) was calculated subtracting each T_m from the control without effector.

Statistical analysis

To compare means, a *t*-test for two independent samples or one-way ANOVA was performed using Minitab 17 statistical software. When comparing kinetic parameters of substrate and effectors curves, the adjusted models were compared with an extra-sum-of-squares *F*-test (Motulsky and Christopoulos, 2003; Hall and Langmead, 2010) using GraphPad Prism (Version 5).

Results

Proteolysis of Ath*PEPCK1 in germinating seedlings*

Transcriptomic data retrieved from the eFP browser (Winter *et al.*, 2007) showed that the expression of *AthPEPCK1* and *AthPEPCK2* in germinating seedlings and mature leaves was considerably different (Supplementary Fig. S1). *AthPEPCK1* transcripts were 620-fold higher than *AthPEPCK2* transcripts in germinating seedlings at 48 hours after imbibition (HAI; Supplementary Fig. S1). *AthPEPCK1* transcripts were 10-fold higher in germinating seedlings at 48 HAI than in mature leaves, while *AthPEPCK2* transcripts were relatively low in germinating seedlings and below the detection limit in mature leaves (Supplementary Fig. S1). Based on this information, our experiments were focused on *Ath*PEPCK1. To analyze the integrity of this protein at different developmental stages, we extracted proteins under denaturing conditions from germinating seedlings harvested at 48 HAI and mature leaves from 32-day-old rosettes (Fig. 1A). *AthPEPCK1* codes for a protein of 73.5 kDa, which further arranges as a hexamer of ~440 kDa (Rojas *et al.*, 2019). We found that *Ath*PEPCK1 was partially proteolyzed in germinating seedlings but not in mature leaves, although the amount of *Ath*PEPCK1 was lower in the latter (Fig. 1A). Some proteases can be active during protein extraction, even with sample buffer containing SDS (Plaxton, 2019). To discard the possibility that *Ath*PEPCK1 from germinating seedlings was degraded during the extraction, we compared four extraction methods, namely sample buffer, sample buffer supplemented with 2 M urea, 10% (w/v) TCA, and 10% (w/v) TCA in acetone. The protocols based on TCA are considered as ultra-denaturing extraction methods. Supplementary Fig. S2A shows that limited proteolysis of *Ath*PEPCK1 occurred *in vivo* and was not an artifact of the extraction procedure. In all our experiments, we found that the majority of *Ath*PEPCK1 was present *in vivo* as a non-proteolyzed form, thus we had to adjust exposure times to visualize the proteolyzed forms (Supplementary Fig. S2B).

Polyclonal antiserum raised against recombinant *Ath*PEPCK1 cross-reacts with *Ath*PEPCK2 (78.4% sequence identity, data not shown). Considering the differences in the relative abundances of *AthPEPCK1* and *AthPEPCK2* transcripts in germinating seedlings (Supplementary Fig. S1), we assumed that the main isoform detected in Fig. 1A was *Ath*PEPCK1. To test our hypothesis, we analyzed protein extracts obtained under denaturing conditions from germinating seedlings of wild-type (WT) plants and the *pck1* knockout mutant. Seedlings were grown under long-day conditions and samples were harvested at time intervals from 4 to 72 HAI. Figure 1B shows that *Ath*PEPCK1 proteolysis peaked at 24–48 HAI in WT plants, whereas no protein bands were detected in the *pck1* mutant at any time point. The proteolysis of *Ath*PEPCK1 was also observed in WT seedlings grown in total darkness (skotomorphogenesis), even though the amount of *Ath*PEPCK1 was significantly lower than in seedlings grown under long-day conditions (Fig. 1B).

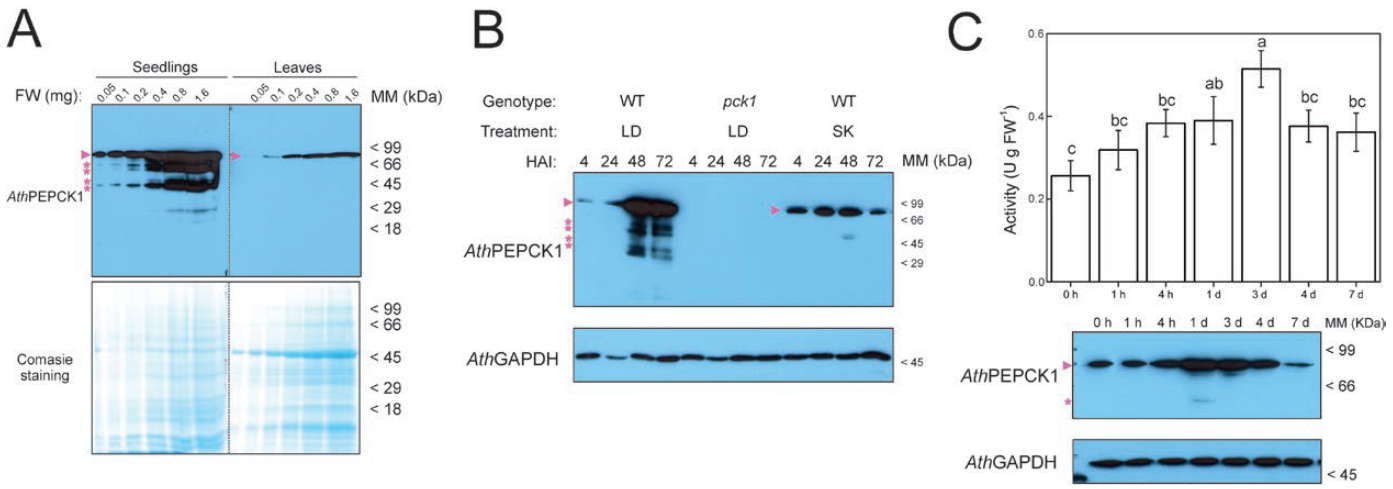

Fig. 1. Proteolysis of *Ath*PEPCK1 in germinating seedlings. (A) Analysis of *Ath*PEPCK1 in germinating seedlings and mature rosettes. Denatured protein extracts from Arabidopsis 48 HAI germinating seedlings (left) and 32-day-old rosettes (right) were resolved by 12% SDS–PAGE (lower panel). Proteins were transferred to nitrocellulose membranes and immunodetected with anti-*Ath*PEPCK1 antiserum (upper panel), as described in the Materials and methods. FW, amount of fresh weight tissue loaded in the gel. (B) Time course of *Ath*PEPCK1 proteolysis during Arabidopsis germination. Western blot performed with anti-*Ath*PEPCK1 antiserum (upper panel) and load control with anti-*Tae*GAPDH antiserum (lower panel) of denatured protein extracts from Arabidopsis seedlings, obtained as described in the Materials and methods. HAI, hours after imbibition; LD, long-day condition (16 h light and 8 h dark); SK, skotomorphogenesis (total darkness). The gel was loaded with 1.3 mg of FW tissue. (C)PEPCK activity in Arabidopsis germinating seedlings. PEPCK carboxylase activity was measured in crude extracts from Arabidopsis seedlings, as described in the Materials and methods. Data are the mean ±SE of four biological replicates. Means that are significantly different (P<0.05) using one-way ANOVA test with a 95% confidence level were grouped with Fisher LSD post-hoc test. In the lower panel, a blot of the measured samples is shown. The gel was loaded with 3 μg of protein. In all the blots, the arrow indicates the full-length *Ath*PEPCK1 and the asterisk its truncated forms.

Based on our results (Fig. 1A, B; Supplementary Fig. S2) and the reports of PEPCK degradation in cucumber cotyledons (Walker *et al.*, 1995), we optimized a protocol for the extraction of native proteins to assess PEPCK activity in germinating seedlings. Extraction was performed with a buffer at pH 9.0 (which diminished PEPCK proteolysis in protein extracts from cucumber; Walker and Leegood, 1995) supplemented with protease inhibitors, to avoid further degradation during the assays. We found that *Ath*PEPCK1 remained stable for at least 4 h after the extraction (Supplementary Fig. S3) and PEPCK activity in crude extracts from Arabidopsis seedlings was in the range described by Malone *et al.* (2007). As shown in Fig. 1C, *Ath*PEPCK1 activity was highest at 72 HAI, while the peak of protein expression was observed at 24 HAI. The maximum level of *Ath*PEPCK1 protein coincided with the onset of proteolysis, at ~24–72 HAI (Fig. 1B, C).

Kinetic and regulatory effects on Ath*PEPCK1 triggered by* Ath*MC9 cleavage*

The multiple *Ath*PEPCK1 bands observed in crude extracts suggested partial proteolysis by a protease (Fig. 1A–C; Supplementary Figs S2, S3). It has been previously reported that *Ath*PEPCK1 was cleaved at the N-terminus by *Ath*MC9 (Tsiatsiani *et al.*, 2013). To test if *Ath*PEPCK1 was cleaved by *Ath*MC9, we incubated recombinant *Ath*PEPCK1 for 60 min with crude extracts from germinating seedlings harvested at 48 HAI at different pH values, as *Ath*MC9 was inactive at alkaline pH (Vercammen *et al.*, 2004). We found that the cleavage of *Ath*PEPCK1 occurred at pH 5.5 and 7.0, whereas it was prevented at pH 9.0 (Fig. 2A).

To analyze the cleavage effect on *Ath*PEPCK1 activity, we cloned the gene coding for *Ath*MC9 from Arabidopsis seedlings and expressed the recombinant protein in *E. coli* cells. Recombinant *Ath*MC9 was expressed as a 37.1 kDa zymogen, which is auto-proteolyzed to produce the p10 (15.4 kDa) and p20 (21.73 kDa) subunits that made up the active *Ath*MC9 (Supplementary Fig. S4; Vercammen *et al.*, 2004). Incubation of *Ath*PEPCK1 with *Ath*MC9 for 1 h completely proteolyzed the former (Fig. 2B). The bands observed in Fig. 2B corresponded to the theoretical fragments predicted according to the *Ath*MC9 recognition sites (K19 and R101; Fig. 2C) (Tsiatsiani *et al.*, 2013). The activity of proteolyzed *Ath*PEPCK1 was slightly higher than that of the full-length protein, although the change was not statistically significant (data not shown).

To further study the effects of *Ath*MC9 cleavage on *Ath*PEPCK1 kinetics, we constructed two N-terminal truncated forms of *Ath*PEPCK1, Δ19 and Δ101. We expressed, purified, and characterized these mutants (Table 1; Supplementary Figs S5, S6). In the carboxylation reaction, the k_{cat} values of the Δ19 and Δ101 truncated enzymes were 1.5- and 1.7-fold higher, respectively, than that of the WT; conversely, all enzymes had similar k_{cat} values in the reaction of decarboxylation (Table 1). Based on K_M values, both mutants had higher apparent affinities for nucleotides (ATP and ADP) and OAA than for PEP, like the WT enzyme (Table 1). The Δ19 mutant showed 2- and 6-fold higher apparent affinity for PEP and OAA, respectively, than the WT. The Δ101 mutant showed 2-fold lower apparent affinity for PEP and 5-fold higher apparent affinity for OAA than the WT. Size exclusion chromatography revealed that both truncated forms were hexamers (Supplementary Fig. S7), like the WT enzyme (Rojas *et al.*, 2019).

Plant PEPCKs are allosterically regulated by metabolites (Hatch and Mau, 1977; Leegood and Ap Rees, 1978; Burnell, 1986; Martín *et al.*, 2011; Rojas *et al.*, 2019). Interestingly, the

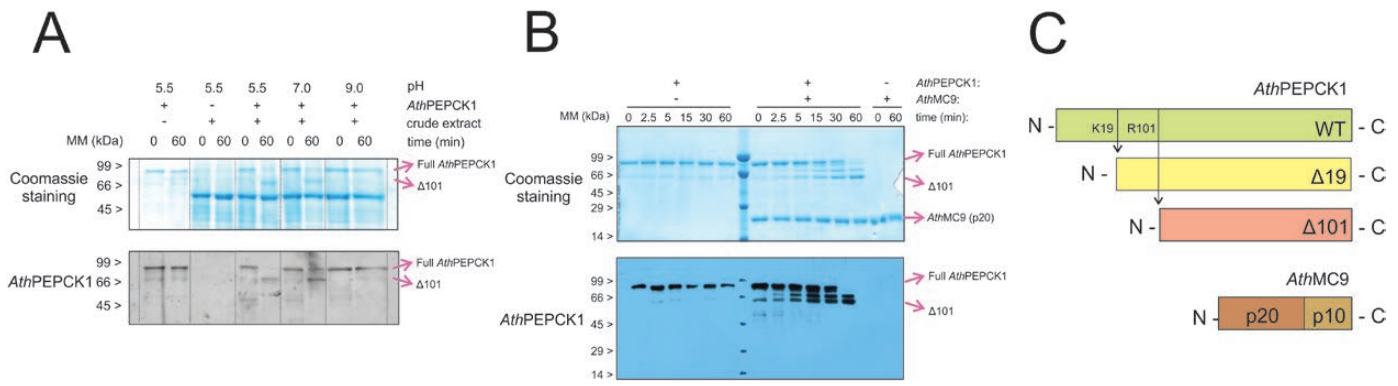

Fig. 2. Analysis of *Ath*PEPCK1 cleavage by *Ath*MC9. (A) Cleavage of *Ath*PEPCK1 by crude extracts from Arabidopsis seedlings. Recombinant *Ath*PEPCK1 was incubated with protein extracts from Arabidopsis seedlings in MES-NaOH pH 5.5, HEPES-NaOH pH 7.0, or Tricine-NaOH pH 9.0 (150 mM in all cases). Reactions were terminated by adding denaturing sample buffer, resolved by 10% SDS–PAGE (upper panel), and immunodetected with anti*Ath*PEPCK1 antiserum (lower panel). The gel was loaded with 0.2 μg of *Ath*PEPCK1 and 2.0 μg of crude extract from 48 HAI seedlings. (B) Proteolysis of *Ath*PEPCK1 by recombinant *Ath*MC9. Reactions were done as described in the Materials and methods, and aliquots were taken at the specified time intervals. Then, samples were resolved by 10% SDS–PAGE (upper panel), transferred to a nitrocellulose membrane, and immunodetected with anti-*Ath*PEPCK1 antiserum (lower panel). The gel was loaded with 1 μg of *Ath*PEPCK1 and 2 μg of *Ath*MC9. (C) Scheme of the *Ath*PEPCK1 truncated mutants constructed according to *Ath*MC9 recognition sites identified by Tsiatsiani *et al.* (2013) and *Ath*MC9 subunits according to Vercammen *et al.* (2004).

Table 1. Kinetic parameters for *Ath*PEPCK1 and truncated mutants

Enzyme	Reaction direction	Substrate	K_M (μM)	K_{cat} (s^{-1})
*Ath*PEPCK1 WT	Carboxylation	PEP[a]	3700±500	1.76±0.04
		ADP[b]	79±15	
	Decarboxylation	OAA[c]	240±20	3.2±0.3
		ATP[d]	66±2	
*Ath*PEPCK1 Δ19	Carboxylation	PEP[e]	1900±400*	2.64±0.06**
		ADP[f]	45±10	
	Decarboxylation	OAA[g]	36±9**	3.38±0.06
		ATP[h]	31±8*	
*Ath*PEPCK1 Δ101	Carboxylation	PEP[i]	7300±700**	3.01±0.08**
		ADP[j]	58±8	
	Decarboxylation	OAA[k]	44±7**	3.9±0.2
		ATP[l]	78±15	

Reactions in both directions of the reaction were performed as described in the Materials and methods. Kinetic constants were calculated by fitting experimental data (Supplementary Figs S5, S6) to the Michaelis–Menten equation and the reported values correspond to the mean ±SE of the adjusted parameters. Comparisons of the parameters were performed with an extra-sum-of-squares *F*-test and the differences are marked with * ($P<0.05$) and ** ($P<0.01$). Fixed substrate concentrations were as follows: [a]0.25 mM ADP, [b]15 mM PEP, [c]0.75 mM ATP, [d]0.75 mM OAA, [e]0.5 mM ADP, [f]5 mM PEP, [g]1.0 mM ATP, [h]0.5 mM OAA, [i]0.5 mM ADP, [j]15 mM PEP, [k]0.5 mM ATP, and [l]0.5 mM OAA. The parameters of the WT enzyme were taken from Rojas *et al.* (2019).

response of the Δ19 and Δ101 mutants to different metabolites was altered compared with the full-length form. Both truncated mutants were more sensitive to PPi than the WT (Fig. 3). Sensitivity to shikimate was slightly increased in the Δ19 mutant compared with the WT (although not statistically significant), while the Δ101 mutant was almost insensitive to this metabolite (Fig. 3). Glc6P inhibited the WT enzyme and the Δ19 truncated form but, surprisingly, the Δ101 truncated form was 2-fold activated by the same metabolite (Fig. 3). Malate activated by 2- and 1.5-fold the WT enzyme and the Δ19 truncated form, respectively, while the Δ101 truncated form was insensitive to this metabolite (Fig. 3). To test whether malate still binds to the Δ101 mutant, we performed thermal shift assays (Rojas *et al.*, 2019). We found that malate produced a similar shift in the melting temperature (T_m) of the WT, Δ19, and Δ101 truncated forms (Fig. 4; Supplementary Fig. S8), suggesting that this metabolite binds to all enzyme forms.

Discussion

The regulation of enzymes by proteolysis is an emergent issue in plant biochemistry. The Arabidopsis genome codes for >800 proteases with distinct temporal and tissue expression profiles (van der Hoorn, 2008; Tsiatsiani *et al.*, 2012), but our knowledge on plant proteolytic cascades is still fragmentary (Paulus and Van der Hoorn, 2019). Understanding the regulation of the gluconeogenic pathway during seed germination is of critical importance, as seedling establishment has a direct impact on plant fitness and productivity (Graham, 2008). Based on this, we focused our studies on the proteolytic regulation of *Ath*PEPCK1, a key regulatory enzyme of plant gluconeogenesis (Penfield *et al.*, 2004, 2012; Eastmond *et al.*, 2015).

Some authors have observed that plant enzymes usually contain N- and C-terminal extensions compared with their bacterial or cyanobacterial counterparts. Such extensions are generally susceptible to post-translational modifications (Lepiniec *et al.*, 1993; Ocheretina *et al.*, 1993; Walker and Leegood, 1995; Furumoto *et al.*, 1999). These extensions might represent regulation modules acquired during evolution to accomplish complex regulations, as plants must respond to ever-changing environmental conditions. The first observation of a discrete proteolytic cleavage at the N-terminus of a plant PEPCK was reported by Walker *et al.* (1995). These authors demonstrated that PEPCK was proteolyzed in crude extracts obtained at neutral pH, which could be prevented by making extractions at alkaline pH (Walker *et al.*, 1995). We found similar results in Arabidopsis, as native extractions at alkaline pH prevented further PEPCK degradation (Fig. 2A; Supplementary Fig. S3). Cleavage of the cucumber PEPCK did not significantly alter its activity (Walker and Leegood, 1995). Therefore, the authors hypothesized that the N-terminal extension would confer unique regulatory properties to the enzyme, not located in the smaller bacterial versions. This model was supported by the fact that plant PEPCK is phosphorylated near the N-terminus, which in turn inhibits the activity of the enzyme (Walker and Leegood, 1995; Leegood and Walker, 1996, 2003; Walker *et al.*, 1997, 2002; Bailey *et al.*, 2007; Chao *et al.*, 2014). The work performed by Shen *et al.* (2017) described a complex activation and inhibition mechanism on *Ath*PEPCK1, depending on the phosphorylated residue. Thus, it would be important to study in detail the kinetic and regulatory properties, as well as the susceptibility to proteolysis, of the phosphorylated enzyme.

In our studies with Arabidopsis seedlings, we found that *Ath*PEPCK1 is subject to proteolysis around 24–48 HAI,

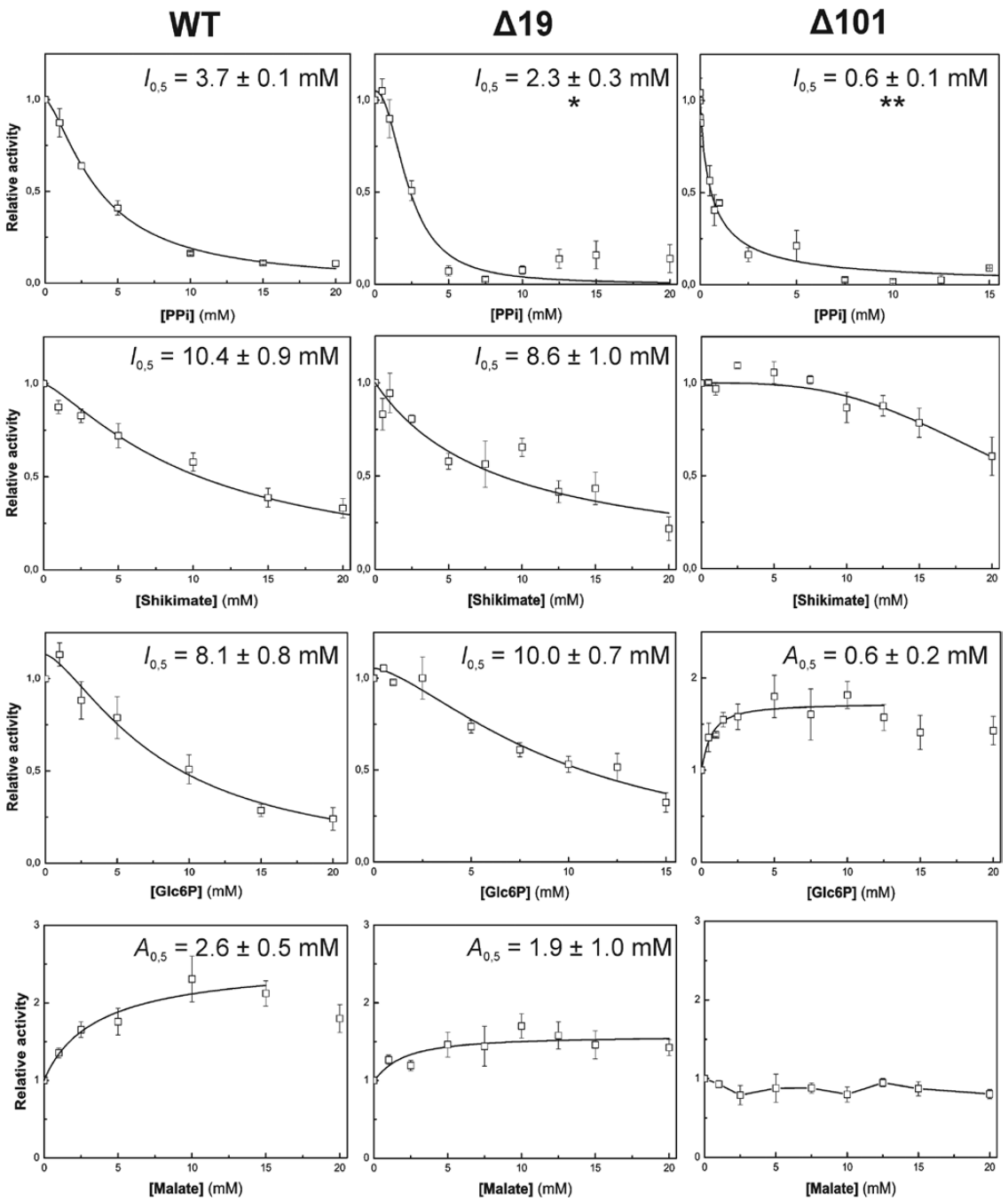

Fig. 3. Analysis of allosteric effectors on *Ath*PEPCKI and truncated mutants. Activity of *Ath*PEPCKI WT (left panel), Δ19 (middle panel), and Δ101 (right panel) was measured in the direction of decarboxylation, as described in the Materials and methods, using the following substrate concentrations: 0.75 mM OAA and 0.75 mM ATP for the WT; and 0.5 mM OAA and 0.3 mM ATP for the Δ19 and Δ101 mutants. In the case of malate, activity was measured in the carboxylation direction using 10 mM PEP and 0.13 mM ADP. Data were fitted to a modified Hill equation and the reported values correspond to the mean ±SE of the adjusted parameters. Comparisons of the parameters were performed with an extra-sum-of-squares *F*-test (*P<0.05, **P<0.01).

when the level of protein reaches a maximum (Fig. 1A–C). To discard the possibility that proteolysis occurs during extraction, we employed ultra-denaturing extraction methods (Supplementary Fig. S2), which confirmed that limited *Ath*PEPCK1 degradation occurs *in vivo*. These findings are in line with the shorter versions of PEPCK found in *A. comosus* leaves extracted with 10% (w/v) TCA (Martín *et al.*, 2011). We measured PEPCK carboxylase activity in these samples, but we did not find the peak of the activity described by Malone *et al.* (2007); instead, we observed a gradual increase of PEPCK

activity (~2-fold), coincident with the peak of protein accumulation (Fig. 1C). These differences might originate from distinct extraction conditions, which might lead to different enzyme populations.

A large-scale study conducted by Tsiatsiani *et al.* (2013) identified *Ath*PEPCK1 as a target of *Ath*MC9. Crude extracts of *mc9* knockout mutants and MC9-overexpressing lines showed decreased and increased PEPCK carboxylase activity, respectively (Tsiatsiani *et al.*, 2013). It is important to note that proteolysis of *Ath*PEPCK1 also occurred in the *mc9* mutant line, probably due to the presence of other metacaspases (such as MC1 and MC4) in this tissue (Tsiatsiani *et al.*, 2013). In this study, the recombinant *Ath*PEPCK1 truncated mutants (Δ19 and Δ101) showed similar decarboxylation activity to the WT enzyme. In comparison, the carboxylation reaction was slightly increased in both truncated forms compared with the WT enzyme (Table 1). The K_M values for the substrates of the truncated mutants were in the same range as those determined for the short version of the pineapple PEPCK (Martín *et al.*, 2011). The K_M for PEP of the Δ19 mutant was 2-fold lower than that of the WT enzyme; similarly, the truncated version of pineapple PEPCK has a 10-fold lower K_M for PEP than the non-proteolyzed enzyme (Daley *et al.*, 1977; Martín *et al.*, 2011).

A key characteristic of the *Ath*PEPCK1 truncated mutants is that allosteric regulation by metabolites differs from that observed for the WT enzyme. In particular, Glc6P is an inhibitor of the WT enzyme, but a weak activator of the Δ101 truncated form, whereas malate activates the WT enzyme and has no effect on the Δ101 truncated form (Fig. 3). These characteristics reinforce the idea that the N-terminal extension confers regulatory properties to plant PEPCK. These results agree with the findings of Furumoto *et al.* (1999), who treated maize PEPCK with enterokinase under controlled conditions to cleave the N-terminus. The proteolyzed enzyme showed 2-fold higher activity and was inhibited by 3-phosphoglyceric acid, while the full-length protein was only slightly affected by this metabolite (Furumoto *et al.*, 1999). In line with our findings, Martín *et al.* (2011) showed that the small version of pineapple PEPCK is not affected by Glc6P or L-malate in the decarboxylation direction of the reaction; unfortunately, we do not know if these metabolites have any effect on the full-length form of the pineapple enzyme, as it could not be purified and characterized (Martín *et al.*, 2011).

The proteolytic regulation of *Ath*PEPCK1 might be part of a mechanism to regulate its levels and/or activity during the sink-to-source transition. During germination, when carbon is obtained from lipids and amino acids, the levels of malate increase, thus activating *Ath*PEPCK1 and the flux of carbon into gluconeogenesis (Fig. 5). Once the photosynthetic apparatus is developed, gluconeogenesis is replaced by glycolysis. At this stage, reduced carbon is obtained from the Benson–Calvin–Basham cycle, the levels of hexose-phosphates increase, and PEPCK activity diminishes ~10-fold, from ~0.5 U g FW^{-1} in germinating seedlings to ~0.05 U g FW^{-1} in mature leaves

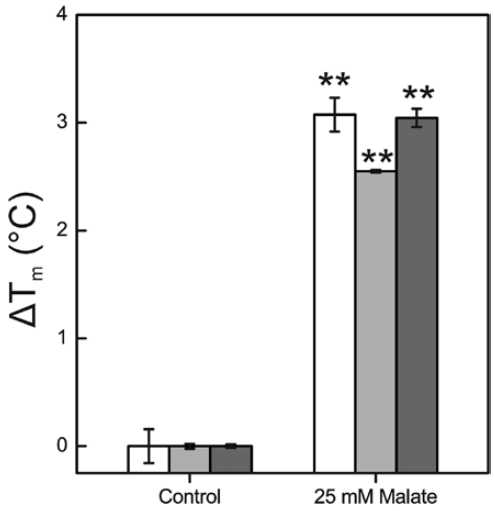

Fig. 4. Thermal shift assays of *Ath*PEPCK1 and truncated mutants. Experiments were performed with the WT (white), Δ19 (light gray), and Δ101 (dark gray) enzymes in control conditions or with 25 mM malate. The shift in the melting temperature (T_m) was calculated as described in the Materials and methods. Data are the mean ±SE of three technical replicates. ** indicates a *P*-value <0.01 using a *t*-test for two independent samples with a confidence level of 95%.

(Fig. 1C; Malone *et al.*, 2007). At this point, *Ath*MC9 might generate the shorter *Ath*PEPCK1 isoforms needed for the new metabolic scenario (Fig. 5). PEPCK is a cataplerotic enzyme that withdraws intermediates of the tricarboxylic acid cycle to maintain their balance under different physiological conditions (Leegood and Walker, 2003), acting in coordination with the anaplerotic enzyme PEP carboxylase (Podestá and Plaxton, 1994; O'Leary *et al.*, 2011). In fact, it has been suggested that the major role played by PEPCK in mammals might be in cataplerosis (Wang and Dong, 2019).

In our experiments, performed with extracts from whole germinating Arabidopsis seedlings, we observed that the majority of *Ath*PEPCK1 remained in the non-proteolyzed form. It is important to note that low-stoichiometry PTM sites could reflect the occurrence of the modification at a specific place and time (Prus *et al.*, 2019). If *Ath*PEPCK1 is differentially regulated in different cell types, then the fraction of proteolyzed isoform would be 'diluted' in the whole seedling extract. Indeed, *AthPEPCK1* expression is differentially regulated in the embryo, the endosperm, and the seed coat of Arabidopsis germinating seeds (Penfield *et al.*, 2004). Similarly, PEPCK from developing pea seeds is differentially expressed in different cell types, but it is only proteolyzed in the cotyledons and the embryonic axis (Delgado-Alvarado *et al.*, 2007). Alternatively, the truncated *Ath*PEPCK1 polypeptides might represent intermediate degradation products during the turnover of the protein in germinating seedlings. It has been reported that such intermediates have a short half-life (Prus *et al.*, 2019), which in turn would lead to an imbalanced stoichiometry with the full-length enzyme.

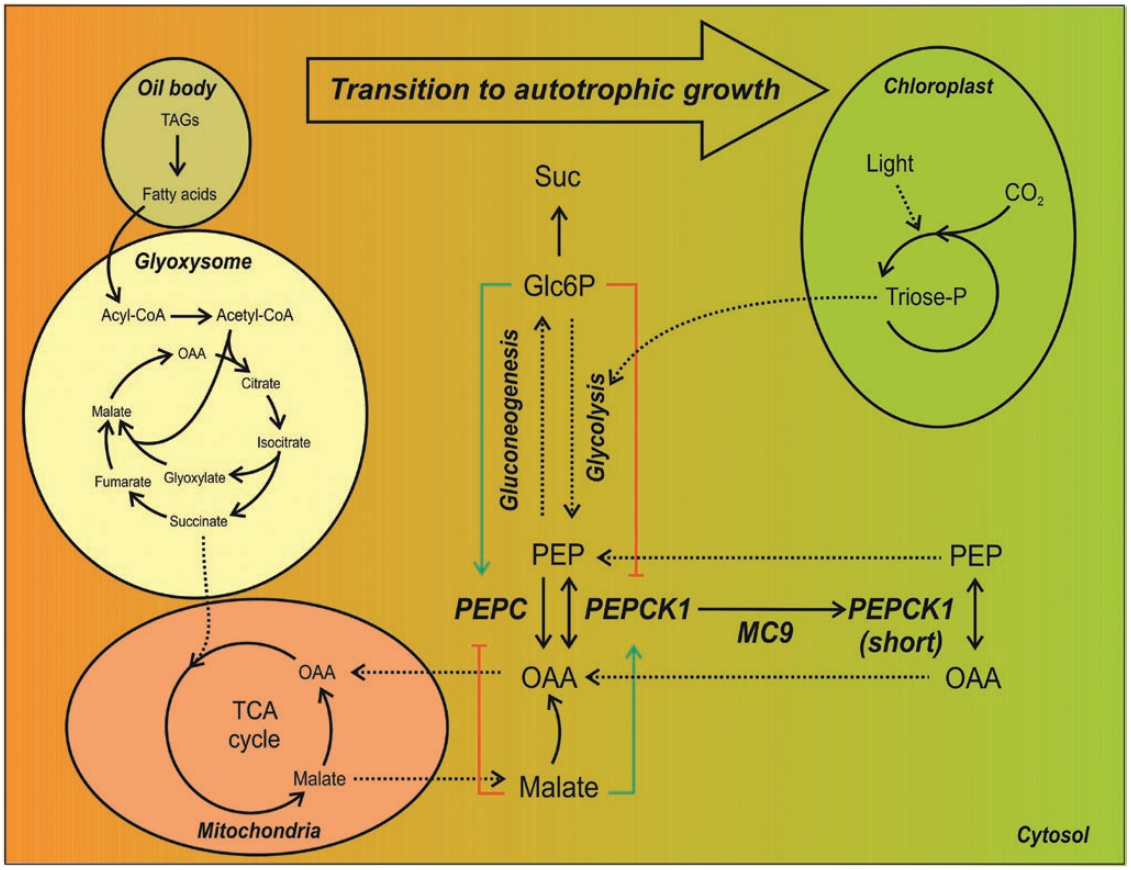

Fig. 5. Regulation of *Ath*PEPCK1 during the sink-to-source transition. During the transition of the seedling from heterotrophic (orange) to autotrophic (green) growth, *Ath*PEPCK1 is cleaved at the N-terminus by *Ath*MC9, leading to shorter enzyme forms, which are catalytic but insensitive to regulation by malate and Glc6P. Green lines, activation; red lines, inhibition.

Actually, it has been shown that *Ath*MC9 generates protein fragments bearing destabilizing residues that could be further processed by the N-end rule pathway (Gibbs *et al.*, 2014, 2016). Experiments to test these hypotheses are currently under way.

Supplementary data

The following supplementary data are available at *JXB* online.

Fig. S1. Comparison of the *AthPEPCK1* and *AthPEPCK2* expression levels.

Fig. S2. Denaturing protein extraction from Arabidopsis leaves and seedlings.

Fig. S3. Native extraction of *Ath*PEPCK1 from germinating seedlings.

Fig. S4. Purification of *Ath*MC9 by IDA-Ni^{2+}.

Fig. S5. Substrate saturation curves for the *Ath*PEPCK1 Δ19 mutant.

Fig. S6. Substrate saturation curves for the *Ath*PEPCK1 Δ101 mutant.

Fig. S7. Size exclusion chromatography for the *Ath*PEPCK1 truncated mutants.

Fig. S8. Thermal shift assay coupled to differential scanning fluorometry for the *Ath*PEPCK1 truncated mutants.

Acknowledgements

This work was supported by grants from ANPCyT (PICT-2017-1515 and PICT-2018-00929 to AAI, and PICT-2018-00865 to CMF) and UNL (CAI+D). CMF is funded by the Max Planck Society (Partner Group for Plant Biochemistry). BER is a Fellow from CONICET; CMF and AAI are Researchers from the same Institution.

Author contributions

Conceptualization, all authors; formal analysis, all authors; funding acquisition, CMF and AAI; investigation, BER and MDH; w
riting—original draft, BER and MDH; writing—review and editing, CMF and AAI.

Data availability

The data that support the findings of this study are openly available in the Dryad Digital Repository at https://doi.org/10.5061/dryad.6t1g1jwww (Rojas *et al.*, 2021).

References

Aich S, Delbaere LTJ. 2007. Phylogenetic study of the evolution of PEP-carboxykinase. Evolutionary Bioinformatics **3**, 333–340.

Bailey KJ, Gray JE, Walker RP, Leegood RC. 2007. Coordinate regulation of phosphoenolpyruvate carboxylase and phosphoenolpyruvate carboxykinase by light and CO_2 during C_4 photosynthesis. Plant Physiology **144**, 479–486.

Bradford MM. 1976. A rapid and sensitive method for the quantitation of microgram quantities of protein utilizing the principle of protein–dye binding. Analytical Biochemistry **72**, 248–254.

Burnell JN. 1986. Purification and properties of phosphoenolpyruvate carboxykinase from C_4 plants. Australian Journal of Plant Physiology **13**, 577–587.

Chao Q, Liu XY, Mei YC, Gao ZF, Chen YB, Qian CR, Hao YB, Wang BC. 2014. Light-regulated phosphorylation of maize phosphoenolpyruvate carboxykinase plays a vital role in its activity. Plant Molecular Biology **85**, 95–105.

Chen ZH, Walker RP, Acheson RM, Leegood RC. 2002. Phosphoenolpyruvate carboxykinase assayed at physiological concentrations of metal ions has a high affinity for CO_2. Plant Physiology **128**, 160–164.

Chen ZH, Walker RP, Acheson RM, Técsi LI, Wingler A, Lea PJ, Leegood RC. 2000. Are isocitrate lyase and phosphoenolpyruvate carboxykinase involved in gluconeogenesis during senescence of barley leaves and cucumber cotyledons? Plant & Cell Physiology **41**, 960–967.

Chiba Y, Kamikawa R, Nakada-Tsukui K, Saito-Nakano Y, Nozaki T. 2015. Discovery of PPi-type phosphoenolpyruvate carboxykinase genes in eukaryotes and bacteria. Journal of Biological Chemistry **290**, 23960–23970.

Choi DS, Kim NH, Hwang BK. 2015. The pepper phosphoenolpyruvate carboxykinase CaPEPCK1 is involved in plant immunity against bacterial and oomycete pathogens. Plant Molecular Biology **89**, 99–111.

Daley LS, Ray TB, Vines HM, Black CC. 1977. Characterization of phosphoenolpyruvate carboxykinase from pineapple leaves *Ananas comosus* (L.) Merr. Plant Physiology **59**, 618–622.

Delgado-Alvarado A, Walker RP, Leegood RC. 2007. Phosphoenolpyruvate carboxykinase in developing pea seeds is associated with tissues involved in solute transport and is nitrogen-responsive. Plant, Cell & Environment **30**, 225–235.

Eastmond PJ, Astley HM, Parsley K, Aubry S, Williams BP, Menard GN, Craddock CP, Nunes-Nesi A, Fernie AR, Hibberd JM. 2015. Arabidopsis uses two gluconeogenic gateways for organic acids to fuel seedling establishment. Nature Communications **6**, 6659.

Edwards GE, Kanai R, Black CC. 1971. Phosphoenolpyruvate carboxykinase in leaves of certain plants whick fix CO_2 by the C_4-dicarboxylic acid cycle of photosynthesis. Biochemical and Biophysical Research Communications **45**, 278–285.

Escamez S, André D, Zhang B, Bollhöner B, Pesquet E, Tuominen H. 2016. METACASPASE9 modulates autophagy to confine cell death to the target cells during Arabidopsis vascular xylem differentiation. Biology Open **5**, 122–129.

Escamez S, Stael S, Vainonen JP, Willems P, Jin H, Kimura S, Van Breusegem F, Gevaert K, Wrzaczek M, Tuominen H. 2019. Extracellular peptide Kratos restricts cell death during vascular development and stress in Arabidopsis. Journal of Experimental Botany **70**, 2199–2210.

Fang L. 2012. Antibody purification from western blotting. Bio-Protocol **2**, e133.

Fukuda W, Fukui T, Atomi H, Imanaka T. 2004. First characterization of an archaeal GTP-dependent phosphoenolpyruvate carboxykinase from the hyperthermophilic archaeon *Thermococcus kodakaraensis* KOD1. Journal of Bacteriology **186**, 4620–4627.

Furumoto T, Hata S, Izui K. 1999. cDNA cloning and characterization of maize phosphoenolpyruvate carboxykinase, a bundle sheath cell-specific enzyme. Plant Molecular Biology **41**, 301–311.

Gibbs DJ, Bacardit J, Bachmair A, Holdsworth MJ. 2014. The eukaryotic N-end rule pathway: conserved mechanisms and diverse functions. Trends in Cell Biology **24**, 603–611.

Gibbs DJ, Bailey M, Tedds HM, Holdsworth MJ. 2016. From start to finish: amino-terminal protein modifications as degradation signals in plants. New Phytologist **211**, 1188–1194.

Goldie AH, Sanwal BD. 1980. Allosteric control by calcium and mechanism of desensitization of phosphoenolpyruvate carboxykinase of *Escherichia coli*. Journal of Biological Chemistry **255**, 1399–1405.

Graham IA. 2008. Seed storage oil mobilization. Annual Review of Plant Biology **59**, 115–142.

Hall DA, Langmead CJ. 2010. Matching models to data: a receptor pharmacologist's guide. British Journal of Pharmacology **161**, 1276–1290.

Hatch MD, Mau S. 1977. Properties of phosphoenolpyruvate carboxykinase operative in C_4 pathway photosynthesis. Functional Plant Biology **4**, 207–216.

Isaacson T, Damasceno CM, Saravanan RS, He Y, Catalá C, Saladié M, Rose JK. 2006. Sample extraction techniques for enhanced proteomic analysis of plant tissues. Nature Protocols **1**, 769–774.

Ito J, Batth TS, Petzold CJ, Redding-Johanson AM, Mukhopadhyay A, Verboom R, Meyer EH, Millar AH, Heazlewood JL. 2011. Analysis of the Arabidopsis cytosolic proteome highlights subcellular partitioning of central plant metabolism. Journal of Proteome Research **10**, 1571–1582.

Johnson TA, Mcleod MJ, Holyoak T. 2016. Utilization of substrate intrinsic binding energy for conformational change and catalytic function in phosphoenolpyruvate carboxykinase. Biochemistry **55**, 575–587.

Kim SM, Bae C, Oh SK, Choi D. 2013. A pepper (*Capsicum annuum* L.) metacaspase 9 (Camc9) plays a role in pathogen-induced cell death in plants. Molecular Plant Pathology **14**, 557–566.

Kwon S Il, Hwang DJ. 2013. Expression analysis of the metacaspase gene family in Arabidopsis. Journal of Plant Biology **56**, 391–398.

Laemmli UK. 1970. Cleavage of structural proteins during the assembly of the head of bacteriophage T4. Nature **227**, 680–685.

Latorre-Muro P, Baeza J, Armstrong EA, Hurtado-Guerrero R, Corzana F, Wu LE, Sinclair DA, López-Buesa P, Carrodeguas JA, Denu JM. 2018. Dynamic acetylation of phosphoenolpyruvate carboxykinase toggles enzyme activity between gluconeogenic and anaplerotic reactions. Molecular Cell **71**, 718–732.e9.

Lea PJ, Chen ZH, Leegood RC, Walker RP. 2001. Does phosphoenolpyruvate carboxykinase have a role in both amino acid and carbohydrate metabolism? Amino Acids **20**, 225–241.

Leegood RC, Ap Rees T. 1978. Phosphoenolpyruvate carboxykinase and gluconeogenesis in cotyledons of *Cucurbita pepo*. Biochimica et Biophysica Acta **524**, 207–218.

Leegood RC, Walker RP. 1996. Phosphorylation of phosphoenolpyruvate carboxykinase in plants. Studies in plants with C_4 photosynthesis and Crassulacean acid metabolism and in germinating seeds. The Biochemical Journal **317**, 653–658.

Leegood RC, Walker RP. 2003. Regulation and roles of phosphoenolpyruvate carboxykinase in plants. Archives of Biochemistry and Biophysics **414**, 204–210.

Lepiniec L, Keryer E, Philippe H, Gadal P, Crétin C. 1993. Sorghum phosphoenolpyruvate carboxylase gene family: structure, function and molecular evolution. Plant Molecular Biology **21**, 487–502.

Malone S, Chen ZH, Bahrami AR, Walker RP, Gray JE, Leegood RC. 2007. Phosphoenolpyruvate carboxykinase in Arabidopsis: changes in gene expression, protein and activity during vegetative and reproductive development. Plant & Cell Physiology **48**, 441–450.

Martín M, Plaxton WC, Podestá FE. 2007. Activity and concentration of non-proteolyzed phosphoenolpyruvate carboxykinase in the endosperm of germinating castor oil seeds: effects of anoxia on its activity. Physiologia Plantarum **130**, 484–494.

Martín M, Rius SP, Podestá FE. 2011. Two phosphoenolpyruvate carboxykinases coexist in the Crassulacean acid metabolism plant *Ananas comosus*. Isolation and characterization of the smaller 65kDa form. Plant Physiology and Biochemistry **49**, 646–653.

Matte A, Tari LW, Goldie H, Delbaere LT. 1997. Structure and mechanism of phosphoenolpyruvate carboxykinase. Journal of Biological Chemistry **272**, 8105–8108.

Motulsky H, Christopoulos A. 2003. Fitting models to biological data using linear and nonlinear regression: a practical guide to curve fitting. San Diego, CA: GraphPad Software Inc.

Ocheretina O, Harnecker J, Rother T, Schmid R, Scheibe R. 1993. Effects of N-terminal truncations upon chloroplast NADP-malate dehydrogenases from pea and spinach. Biochimica et Biophysica Acta **1163**, 10–16.

O'Leary B, Park J, Plaxton WC. 2011. The remarkable diversity of plant PEPC (phosphoenolpyruvate carboxylase): recent insights into the physiological functions and post-translational controls of non-photosynthetic PEPCs. The Biochemical Journal **436**, 15–34.

Paulus JK, Van der Hoorn RAL. 2019. Do proteolytic cascades exist in plants? Journal of Experimental Botany **70**, 1997–2002.

Penfield S, Clements S, Bailey KJ, Gilday AD, Leegood RC, Gray JE, Graham IA. 2012. Expression and manipulation of PHOSPHOENOLPYRUVATE CARBOXYKINASE 1 identifies a role for malate metabolism in stomatal closure. The Plant Journal **69**, 679–688.

Penfield S, Rylott EL, Gilday AD, *et al.* 2004. Reserve mobilization in the Arabidopsis endosperm fuels hypocotyl elongation in the dark, is independent of abscisic acid, and requires PHOSPHOENOLPYRUVATE CARBOXYKINASE1. The Plant Cell **16**, 2705–2718.

Piattoni CV, Ferrero DML, Dellaferrera I, Vegetti A, Iglesias AÁ. 2017. Cytosolic glyceraldehyde-3-phosphate dehydrogenase is phosphorylated during seed development. Frontiers in Plant Science **8**, 522.

Plaxton WC. 2019. Avoiding proteolysis during the extraction and purification of active plant enzymes. Plant & Cell Physiology **60**, 715–724.

Podestá FE, Plaxton WC. 1994. Regulation of cytosolic carbon metabolism in germinating *Ricinus communis* cotyledons. Planta **194**, 374–380.

Prus G, Hoegl A, Weinert BT, Choudhary C. 2019. Analysis and interpretation of protein post-translational modification site stoichiometry. Trends in Biochemical Sciences **44**, 943–960.

Raineri J, Hartman MD, Chan RL, Iglesias AA, Ribichich KF. 2016. A sunflower WRKY transcription factor stimulates the mobilization of seed-stored reserves during germination and post-germination growth. Plant Cell Reports **35**, 1875–1890.

Reiskind JB, Bowes G. 1991. The role of phosphoenolpyruvate carboxykinase in a marine macroalga with C_4-like photosynthetic characteristics. Proceedings of the National Academy of Sciences, USA **88**, 2883–2887.

Rojas BE, Hartman MD, Figueroa CM, Leaden L, Podestá FE, Iglesias AA. 2019. Biochemical characterization of phospho enol pyruvate carboxykinases from *Arabidopsis thaliana*. The Biochemical Journal **476**, 2939–2952.

Rojas BE, Hartman MD, Figueroa CM, Iglesias AA. 2021. Data from: Proteolytic cleavage of *Arabidopsis thaliana* phosphoenolpyruvate carboxykinase-1 modifies its allosteric regulation. Dryad Digital Repository https://doi.org/10.5061/dryad.6t1g1jwww.

Rylott EL, Gilday AD, Graham IA. 2003. The gluconeogenic enzyme phosphoenolpyruvate carboxykinase in Arabidopsis is essential for seedling establishment. Plant Physiology **131**, 1834–1842.

Sáez-Vásquez J, Raynal M, Delseny M. 1995. A rapeseed cold-inducible transcript encodes a phosphoenolpyruvate carboxykinase. Plant Physiology **109**, 611–618.

Saito T, Matsukura C, Ban Y, Shoji K, Sugiyama M, Fukuda N, Nishimura S. 2008. Salinity stress affects assimilate metabolism at the gene-expression level during fruit development and improves fruit quality in tomato (*Solanum lycopersicum* L.). Journal of the Japanese Society for Horticultural Science **77**, 61–68.

Shen W, Liu J, Li JF. 2019. Type-II metacaspases mediate the processing of plant elicitor peptides in Arabidopsis. Molecular Plant **12**, 1524–1533.

Shen Z, Dong XM, Gao ZF, Chao Q, Wang BC. 2017. Phylogenic and phosphorylation regulation difference of phosphoenolpyruvate carboxykinase of C_3 and C_4 plants. Journal of Plant Physiology **213**, 16–22.

Tsiatsiani L, Gevaert K, Van Breusegem F. 2012. Natural substrates of plant proteases: how can protease degradomics extend our knowledge? Physiologia Plantarum **145**, 28–40.

Tsiatsiani L, Timmerman E, De Bock PJ, *et al.* 2013. The Arabidopsis metacaspase9 degradome. The Plant Cell **25**, 2831–2847.

van der Hoorn RAL. 2008. Plant proteases: from phenotypes to molecular mechanisms. Annual Review of Plant Biology **59**, 191–223.

Vercammen D, Belenghi B, van de Cotte B, Beunens T, Gavigan JA, De Rycke R, Brackenier A, Inzé D, Harris JL, Van Breusegem F. 2006. Serpin1 of *Arabidopsis thaliana* is a suicide inhibitor for metacaspase 9. Journal of Molecular Biology **364**, 625–636.

Vercammen D, van de Cotte B, De Jaeger G, Eeckhout D, Casteels P, Vandepoele K, Vandenberghe I, Van Beeumen J, Inzé D, Van Breusegem F. 2004. Type II metacaspases Atmc4 and Atmc9 of *Arabidopsis thaliana* cleave substrates after arginine and lysine. Journal of Biological Chemistry **279**, 45329–45336.

Walker RP, Acheson RM, Tecsi LI, Leegood RC. 1997. Phosphoenolpyruvate carboxykinase in C_4 plants: its role and regulation. Australian Journal of Plant Physiology **24**, 459–468.

Walker RP, Chen ZH, Acheson RM, Leegood RC. 2002. Effects of phosphorylation on phosphoenolpyruvate carboxykinase from the C_4 plant Guinea grass. Plant Physiology **128**, 165–172.

Walker RP, Chen ZH, Tecsi LI, Famiani F, Lea PJ, Leegood RC. 1999. Phosphoenolpyruvate carboxykinase plays a role in interactions of carbon and nitrogen metabolism during grape seed development. Planta **210**, 9–18.

Walker RP, Leegood RC. 1995. Purification, and phosphorylation in vivo and in vitro, of phosphoenolpyruvate carboxykinase from cucumber cotyledons. FEBS Letters **362**, 70–74.

Walker RP, Trevanion SJ, Leegood RC. 1995. Phosphoenolpyruvate carboxykinase from higher plants: purification from cucumber and evidence of rapid proteolytic cleavage in extracts from a range of plant tissues. Planta **196**, 58–63.

Wang Z, Dong C. 2019. Gluconeogenesis in cancer: function and regulation of PEPCK, FBPase, and G6Pase. Trends in Cancer **5**, 30–45.

Winter D, Vinegar B, Nahal H, Ammar R, Wilson GV, Provart NJ. 2007. An 'Electronic Fluorescent Pictograph' browser for exploring and analyzing large-scale biological data sets. PLoS One **2**, e718.

Wu FS, Wang MY. 1984. Extraction of proteins for sodium dodecyl sulfate–polyacrylamide gel electrophoresis from protease-rich plant tissues. Analytical Biochemistry **139**, 100–103.